J Comput Neurosci
DOI 10.1007/s10827-013-0482-4

The role of dendritic spine morphology in the compartmentalization and delivery of surface receptors

Cory M. Simon · Iain Hepburn · Weiliang Chen · Erik De Schutter

Received: 16 July 2013 / Revised: 10 September 2013 / Accepted: 24 September 2013

Abstract Since AMPA receptors are major molecular players in both short- and long-term plasticity, it is important to identify the time-scales of and factors affecting the lateral diffusion of AMPARs on the dendrite surface. Using a mathematical model, we study how the dendritic spine morphology affects two processes: (1) compartmentalization of the surface receptors in a single spine to retain local chemistry and (2) the delivery of receptors to the post-synaptic density (PSD) of spines via lateral diffusion following insertion onto the dendrite shaft. Computing the mean first passage time (MFPT) of surface receptors on a sample of real spine morphologies revealed that a constricted neck and bulbous head serve to compartmentalize receptors, consistent with previous works. The residence time of a Brownian diffusing receptor on the membrane of a single spine was computed to be ~ 5 s. We found that the location of the PSD corresponds to the location at which the maximum MFPT occurs, the position that maximizes the residence time of a diffusing receptor. Meanwhile, the same geometric features of the spine that compartmentalize receptors inhibit the recruitment of AMPARs via lateral diffusion from dendrite insertion sites. Spines with narrow necks will trap a smaller fraction of diffusing receptors in the their PSD when considering competition for receptors between the spines, suggesting that ideal geometrical features involve a tradeoff depending on the intent of compartmentalizing the current receptor pool or recruiting new AMPARs in the PSD. The ultimate distribution of receptors among the spine PSDs by lateral diffusion from the dendrite shaft is an interplay between the insertion location and the shape and locations of both the spines and their PSDs. The time-scale for delivery of receptors to the PSD of spines via lateral diffusion was computed to be ~ 60 s.

Keywords AMPA receptors · Surface receptors · Mean first passage time · Surface diffusion

Action Editor: Arnd Roth

C. M. Simon (✉)
Department of Chemical and Biomolecular Engineering, University of California, Berkeley, CA, USA
e-mail: corymsimon@gmail.com

I. Hepburn · E. De Schutter
Theoretical Neurobiology, University of Antwerp, Antwerp, Belgium

I. Hepburn · W. Chen · E. De Schutter
Computational Neuroscience Unit, Okinawa Institute of Science and Technology, Onna-son, Okinawa, Japan

Introduction

Glutamate is the major neurotransmitter that mediates communication between the excitatory synapses of a pre- and post-synaptic neuron (Sheng and Lee 2001). The glutamate receptor of the AMPA type (AMPAR) is a ligand-gated ion channel that resides in the membrane and responds to glutamate binding by opening its pore. The molecular basis for synaptic plasticity processes important in learning, such as long-term potentiation (LTP), is believed to depend on the number of AMPARs in the synapse (OBrien et al. 1998; Lynch and Baudry 1984; Choquet 2010).

The fluid mosaic model of biological membranes (Singer and Nicolson 1972) does not preclude surface receptors from diffusing out of the synaptic region or spine in the absence of scaffolding proteins, cytoskeletal structures, or other diffusion obstacles that hold

Published online: 10 October 2013

them in place (Choquet 2010). Although such scaffolding mechanisms exist to help localize AMPARs at the synapse (Sheng and Jong Kim 2002; Opazo et al. 2010), fluorescence recovery after photobleaching (FRAP) (Jaskolski and Henley 2009) experiments indicated that 50 % of GluR2-AMPARs are mobile in the spine head (Ashby et al. 2006). Single-particle tracking using quantum dots indicated that 70 % of GluR1-AMPARs were mobile in the post-synaptic membrane (but half of this population was confined to the postsynaptic density) (Heine et al. 2008). Further, AMPARs laterally diffuse at rates significant enough to affect synaptic activity over the time scales of glutamate release by the presynaptic neuron, allowing lateral diffusion to play a role in reducing paired-pulse depression by replenishing the pool of desensitized receptors between firings (Heine et al. 2008). It is thus important to identify the time-scales of and factors affecting the lateral movement of receptors.

For a spine to act as a discrete unit, it must retain its local chemistry distinct from its shaft and adjacent spines over the communication timescale by compartmentalizing receptors (Svoboda et al. 1996). The typical dendritic spine has a narrow neck connecting a bulbous head to the dendrite, and this morphology compartmentalizes diffusing intracellular molecules in (Santamaria et al. 2006; Sabatini et al. 2001; Holmes 1990; Noguchi et al. 2005; Svoboda et al. 1996) and receptors on (Ashby et al. 2006; Hugel et al. 2009) spines. Theoretical models elucidate how geometric parameters, such as a narrow spine neck, affect the confinement time of diffusing molecules in/on the spine (Holcman et al. 2005; Biess et al. 2007; Schuss et al. 2007; Holcman and Schuss 2011; Santamaria et al. 2006). The spine shape is dynamic in time (Fischer et al. 1998), and the possibility remains that the spine shape is regulated to control synaptic plasticity by altering the compartmentalization of molecules.

In Part I, we build upon previous works to address how the spine morphology itself plays a role in compartmentalizing AMPARs diffusing on the membrane. A metric for how the spine acts as a distinct, isolated reactor or compartment is Dynkin's mean first passage time (MFPT)– the mean time a diffusing surface receptor first exits the spine (Schuss 1980). Most modeling work on the MFPT in the dendritic spine idealizes spine geometry or relies on asymptotically thin spine necks in order to write analytical formulas, providing insight into how features of the spine geometry compartmentalize molecules. A collection of analytical results for idealized geometries is found in (Holcman and Schuss 2011), where it is shown that the MFPT is highly sensitive to the connection between the spine neck and head. In this work, we use a finite volume method to compute the MFPT of surface receptors on mesh reconstructions of microscope images (Harris 2012) of real dendritic spines (see Fig. 1a). Along with quantifying the degree to which real spine geometries compartmentalize their chemistry, we investigate how different geometric features affect the MFPT. We compare the location at which the maximum MFPT occurs to the location of the excitatory synapse (see Fig. 1a) to see if the synapse is located in a position that maximizes compartmentalization potential.

Surface diffusion of AMPARs plays an important role in the LTP process in two ways (Makino and Malinow 2009). Firstly, AMPA receptors that incorporate into the PSD during LTP induction are recruited mostly from local, extrasynaptic spine membrane regions by lateral diffusion. Secondly, GluR1-containing AMPARs that are delivered primarily to the surface of the dendritic shaft by exocytosis then laterally diffuse from the dendritic shaft into nearby spines (Choquet and Triller 2003) to gradually replenish local pools of extrasynaptic receptors. The surface delivery of AMPARs was visualized in (Yudowski et al. 2007). These authors did not observe direct exocytotic insertion onto the spine, underscoring that AMPARs are delivered to synapses by lateral diffusion from the dendritic shaft. The number of AMPARs in the synapse is very low and highly variable (38±34 in Purkinje cell synapses (Masugi-Tokita et al. 2007), 10-20 per synapse in CA1 pyramidal neurons (Nicholson et al. 2006)), so it is important to consider the effects of freshly inserted receptors.

Part II concerns the delivery of surface receptors to the excitatory synapses of spines via lateral diffusion after insertion onto the dendritic shaft. We simulate the diffusion of a receptor that was inserted onto the dendritic shaft on a mesh reconstruction of a dendrite morphology with 21 spines with known PSD locations. We compute the time it

Fig. 1 **a** Dendrite K21 reconstruction with multiple spines. Excitatory postsynaptic density shown in red. **b** An individual spine cut from the dendrite on which we compute the MFPT (mathematically represented as Ω_s)

takes for the receptor to reach the PSD of a spine, modeled as a trapping region, and the probability that a particular spine PSD will receive the receptor. We address the following questions; the first is a question of precision and the second is a question of imprecision. (1) How does the location of a single AMPAR insertion site affect the probability that AMPARs from that site will be delivered to a particular nearby spine? (2) For an ensemble of random insertion sites, how is the final distribution of AMPARs among spines affected by the spine geometry?

1 Materials and methods

1.1 The triangular mesh representation of the dendrite, spines, and excitatory synaptic regions

Surface mesh reconstructions of images of real dendritic spines (from CA1 stratum radiatum series K21 and K18) were downloaded from (Harris 2012) as VRML objects, and non-manifold vertices were manually repaired in Blender, an open-sourced software for 3D computer graphics. For part I, Blender was used to manually cut the spines from the dendrite for simulation of the MFPT PDE in Eq. (12) on the surface. A total of 33 spines were used (14 from dendrite K21 and 19 from dendrite K18). For part II, Blender was used to manually cut the triangles intersecting with the synaptic regions (in red Fig. 1a) from the dendrite K21 for the zero boundary condition on Ω_{PSD}. Gmsh (Geuzaine and Remacle 2009) was used to convert the .stl files from Blender into .gmsh files that were imported into Python using FiPy (Guyer et al. 2009), a finite volume package. FiPy was not used for implementing the finite volume method, but the built-in MayAvi2 viewer was used for visualizing the data (e.g., Fig. 4 heat maps and Fig. 7 dendrite images). Dendrite K21 and an extracted spine is in Fig. 1a and b, respectively. The dendrite K21 has excitatory synaptic regions indicated in red and was first published in (Harris and Stevens 1989).

1.2 The finite volume method for solving PDEs on the surface mesh

The NumPy and SciPy packages in Python(x,y) were used to build and solve the resulting matrix system from the finite volume method and the matplotlib package was used for plotting.

1.2.1 Part I: The poisson equation

We seek to approximate the solution to Eq. (11) on a surface that is approximated by a triangular mesh of n ordered triangles. We denote a triangular face j as A_j with corresponding edges $f_{j,i}$ for $i = 1, 2, 3$ and centers c_j. Thus we have that Ω_s is represented by $A_1 \cup A_2 \cup ... \cup A_n$. The finite volume method involves the variables:

$$T_j := \int_{A_j} \bar{\tau}_{(y)} dS_x. \tag{1}$$

We integrate Eq. (11) over each surface triangle A_j and apply Green's identity to get:

$$\sum_{i=1}^{3} \int_{f_{j,i}} \nabla_s \bar{\tau}_{(y)} \cdot n_{j,i} dl_{\mathbf{x}} = -\frac{|A_j|}{D}, \tag{2}$$

where $n_{j,i}$ is the outward normal vector to triangle j across edge $f_{j,i}$. We choose to approximate the flux across each edge as uniform across the edge to bring in the unknowns T_j:

$$\int_{f_{j,i}} \nabla_s \bar{\tau}_{(y)} \cdot n_{j,i} dl_{\mathbf{x}} \approx \frac{|f_{j,i}|}{|c_j - c_{a(j,i)}|} \left(\frac{T_{a(j,i)}}{|A_{a(j,i)}|} - \frac{T_j}{|A_j|} \right), \tag{3}$$

where, for notational convenience, we define the function $a(j, i)$ for $i = 1, 2, 3$ to give the index of the adjacent triangle corresponding to face $f_{j,i}$. The above approximation for the gradient yields a consistent numerical scheme when the mesh is a Voronoi mesh (Kieri 2011), since then the line between the centers of two adjacent triangles is orthogonal to the shared face. In the absence of a Voroni mesh, when the said orthogonality condition does not hold, it is shown in (Cautres et al. 2004) that the method of using only the two values T_j and $T_{a(j,i)}$ to approximate the flux across the faces (as above) converges with at least order 1/2. To incorporate the zero boundary condition, we define $T_{a(j,i)}$ if $a(j, i)$ corresponds to a boundary vertex and use the closest distance from c_j to the boundary vertex in place of $|c_j - c_{a(j,i)}|$.

Using the expression for the flux in Eq. (3), Eq.(2) is a linear system of N equations to solve for T_j. Solving the matrix system, we then find the approximate value of $\bar{\tau}_{(y)}$ on each triangle as $\frac{T_j}{|A_j|}$.

1.2.2 Part II: The surface diffusion equation

To simulate the time-dependent diffusion Eq. (16), we use the same spatial discretization as above and use a first order approximation for the time derivative, treating the Laplacian implicitly in time. We denote $P_j^k := \int_{A_j} p(x, j\Delta t) dS_x$ and the finite volume discretization becomes:

$$\frac{P_j^k - P_j^{k-1}}{\Delta t} = \sum_{i=1}^{3} \frac{|f_{j,i}|}{|c_j - c_{a(j,i)}|} \left(\frac{D_{a(j,i)} P_{a(j,i)}^k}{|A_{a(j,i)}|} - \frac{D_j P_j^k}{|A_j|} \right). \tag{4}$$

This can be written as a matrix system to solve for $P^k := [P_1^k, P_2^k, ..., P_N^k]$ at each time step when N cells are involved: $JP^k = P^{k-1}$. Row i of J corresponds to the

conservation equation written for cell i, and the entries are computed by looping over the (maximally) three adjacent cells to cell i.

Integral (17) is approximated by considering the zero value of p in Ω_{PSD}:

$$f_j(t_k) \approx f_j(t_{k-1}) + \sum_{i:\text{triangles bordering } \Omega_{PSD,j}} D\frac{P_i^k}{|l_i||A_i|}|f_{i,a(i)}|\Delta t, \tag{5}$$

where $a(i)$ maps the triangle index i to the face $f_{i,a(i)}$ that composes $\Omega_{PSD,j}$ and l_i is the shortest distance from c_i to the face $f_{i,a(i)}$.

1.3 Sphere-cylinder least squares fitting to point cloud spine representation

Here we have a point cloud $P = \{x_i \in \mathbb{R}^3 | i = 1, 2, ..., N\}$, chosen to be the triangulated mesh vertices, that represents the spine, and we seek to fit a sphere (radius R_s and center $c_s \in \mathbb{R}^3$) and orthogonally intersecting cylinder (axis direction $e \in \mathbb{R}^3$ and radius R_c) to the point set. We partition the point cloud into two sets S and C such that $S \cup C = P$ and $S \cap C = \emptyset$. The intention is to group the points together in S (C) that are best-approximated by the sphere (cylinder orthogonal to the sphere). We use a least-squares algorithm for fitting a sphere and cylinder to S and C, respectively, and a clustering algorithm to determine the best partition. The algorithm is to recursively follow these steps until the assignment of points to partitions does not change:

1. Fit a sphere to the points in S using a least-squares criterion.
2. Fit a cylinder orthogonal to the sphere from step 1 to the points in C using a least-squares criterion.
3. For each point in P, compute the nearest distance to the best-fit sphere, d_s and to the best-fit cylinder, d_c. If $d_c < d_s$, assign the point to the set C, otherwise assign the point to the set S.

1.3.1 Fitting a sphere to n_s points in S

The optimization problem is:

$$\min_{R_s, c_s} \sum_{i:x_i \in S} (||x_i - c_s|| - R_s)^2, \tag{6}$$

and upon setting the derivatives with respect to R_s and c_s to zero, we get:

$$R_s = \frac{1}{n_s} \sum_{i:x_i \in S} ||x_i - c_s|| \tag{7}$$

$$c_s = \frac{1}{n_s} \sum_{i:x_i \in S} x_i \tag{8}$$

1.3.2 Fitting a cylinder to n_c points in C

Let us denote the primary axis of the cylinder as the line parameterized by t: $r(t) = c_s + et$, where $||e|| = 1$. Finding the point on the primary axis $r(t^*)$ that is closest to x_i, we find $t^* = e^T(x_i - c_s)$. The optimization problem is then to find the primary axis that minimizes the sum of distances between x_i and the primary axis:

$$\min_{e:||e||=1} \sum_{i:x_i \in C} ||x_i - (c_s + e^T(x_i - c_s)e)||^2, \tag{9}$$

which we can rewrite by using the scatter matrix $A = \sum_{i:x_i \in C} (x_i - c_s)(x_i - c_s)^T$:

$$\min_{e:||e||=1} -e^T A e + \sum_{i:x_i \in C} ||x_i - c_s||^2. \tag{10}$$

The second term is fixed, and we must maximize $e^T Ae$ such that $||e|| = 1$. Since A is a symmetric matrix (assumed full rank), we have that any vector in $\mathbb{R}^3$ can be expressed as a linear combination of the eigenvectors of A, and one can show that the maximum of $e^T Ae$ (s.t. e is a unit vector) occurs when e is the the eigenvector of A corresponding to the highest eigenvalue. We then take R_c as the average of the distances of x_i to the primary axis determined by $c_s + te$.

2 Part I: The role of dendritic spine morphology in compartmentalizing surface receptors

2.1 The model

While we model receptor movement as spatially uniform Brownian motion, the actual movement of AMPA receptors on the spine surface is more complicated. AMPARs "halt regularly and reversibly in confinement zones, mostly corresponding to reversible arrest near synaptic structures, but sometimes also originating from arrest in endocytic pits and from spontaneous neuronal activity" (Borgdorff and Choquet 2002). Reported diffusion coefficients of AMPARs are 0.0798 μm^2/s outside the synapse and 0.0153 μm^2/s inside the synapse (Renner et al. 2009) (Hippocampal neurons from 18-day-old Sprague Dawley rat embryos), in rough agreement with a histogram of diffusion coefficients from single particle tracking experiments in (Heine et al. 2008) (CA1 pyramidal neurons from hippocampal slices and in cultured hippocampal neurons).

We seek to extract the effects of the spine shape on the lateral diffusion of receptors from among the other factors that help compartmentalize AMPARs at the spine– scaffolding proteins, lipid rafts, and trafficking (Ehlers et al. 2007; Newpher and Ehlers 2008)– by a judicious choice of our Brownian diffusion coefficient. We take the measurement

of the diffusion coefficient outside the synapse, 0.08 $\mu m^2/s$, where quantum dot experiments reveal AMPARs are freely moving (Renner et al. 2009). We neglect the trafficking of AMPARs on and off of the spine under the justification that most exocytosis from internal cellular compartments occurs on the dendritic shaft outside of the spine (Makino and Malinow 2009). Any discrepancy between our computed MFPT of a freely diffusing receptor and experiment is thus due to the scaffolding/trapping of receptors. The MFPT we proceed to compute is a lower bound, and it reflects only the effect of spine shape, as intended.

For a diffusing surface receptor on the spine membrane $\Omega_s \subset \mathbb{R}^3$, the first passage time problem asks the following question: given an initial position y of a diffusing receptor on a surface, what is the time $\tau_{(y)}$ the receptor takes to first exit the spine Ω_s (Fig. 2)? While $\tau_{(y)}$ is a random variable, the mean first passage time $\bar{\tau}_{(y)}$ is the solution to a Poisson equation when the diffusion coefficient is spatially homogeneous (Dyhkin 1965; Schuss 1980):

$$\Delta_{s,y}\bar{\tau}_{(y)} = -\frac{1}{D},\ y \in \Omega_s \tag{11}$$

$$\bar{\tau}_{(y)} = 0,\ y \in \partial\Omega_s, \tag{12}$$

where Δ_s is the surface Laplacian or the Laplace-Beltrami operator ((Calhoun and Helzel 2009) for an accessible description), and y is the initial position of the particle. The subscript y emphasizes that $\tau_{(y)}$ is a function of the initial condition y. The confinement time is an average of the mean first passage times over all possible initial conditions y (Holcman and Schuss 2004):

$$T = \frac{1}{|\Omega_s|}\int_{\Omega_s} \bar{\tau}_{(y)} dS_y. \tag{13}$$

The confinement time is a useful scalar metric for quantifying how a spine acts as a distinct reactor or compartment for a receptor. It is a function of the geometry and the diffusion coefficient D of the receptor. Another scalar metric for compartmentalization is the maximum of $\tau_{(y)}$ over all initial conditions, which we will explore.

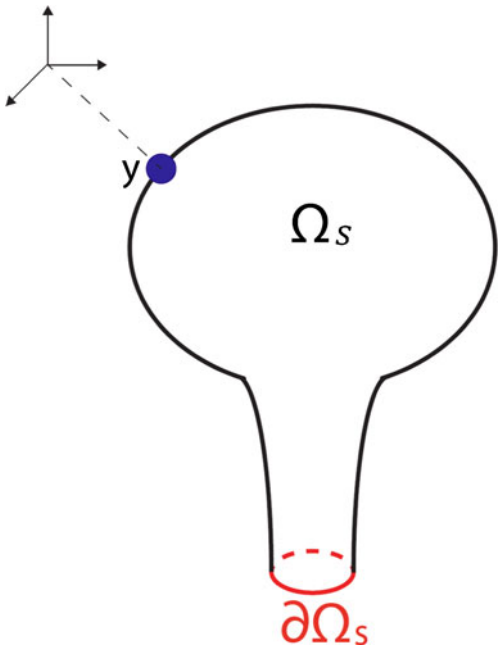

Fig. 2 Mean first passage time illustration. Given a particle with an initial position y on the surface domain Ω_s, what is the mean time that it takes for the particle to first reach $\partial\Omega_s$? Here, Ω_s is chosen to be the spine surface so that reaching $\partial\Omega_s$ is equivalent to exiting the spine

2.2 Results

We numerically solved Eq. (12) (with $D = 0.08\ \mu m^2/s$) on a sample of 33 mesh reconstructions of dendritic spines (see Materials and Methods). We computed the median confinement time to be 4.02 s, and the median maximum MFPT to be 6.4 s. This gives a time scale over which receptors retain residence on the spine in the absence of lipid rafts or cytoskeletal structures that interfere with the lateral diffusion of receptors, isolating the geometry as a parameter in the degree of compartmentalization. Next, we computed from the mesh reconstructions three spine geometry descriptors: the surface area, the circumference of the opening onto the dendrite, and the greatest distance of a point on the spine surface from the center of the opening onto the dendrite (a measure of length).

First, we investigated the relationship between confinement times and the surface area of spines. For a given spine neck circumference, we expect large surface areas to endow spines with large confinement times because the receptors must explore a greater region to find the spine exit. This general trend is present in Fig. 3a, a surface area-confinement time scatter plot. By comparing two points with the same surface area, but different confinement times, and visa-versa, we can gain insight into how the spine shape affects the compartmentalization of the receptors. The two spines K21.1 (red) and K21.3 (yellow) have similar surface areas, but K21.1 has a much higher confinement time. This can be explained by the thinner spine neck for K21.1 that acts as a restriction for the particle to exit. The two spines K21.6 (pink) and K21.2 (green) have similar confinement times, but K21.2 has a greater surface area. The fact that spine K21.6 can achieve the same degree of compartmentalization as K21.2 with less surface area is due to its constricted neck which at its narrowest point is much narrower than spine K21.2.

We also observe a correlation between the confinement time and the greatest distance from the center of the spine opening in Fig. 3b. For a fixed spine neck radius, a longer spine will generally be endowed with a higher confinement time because the receptor must travel a greater distance to

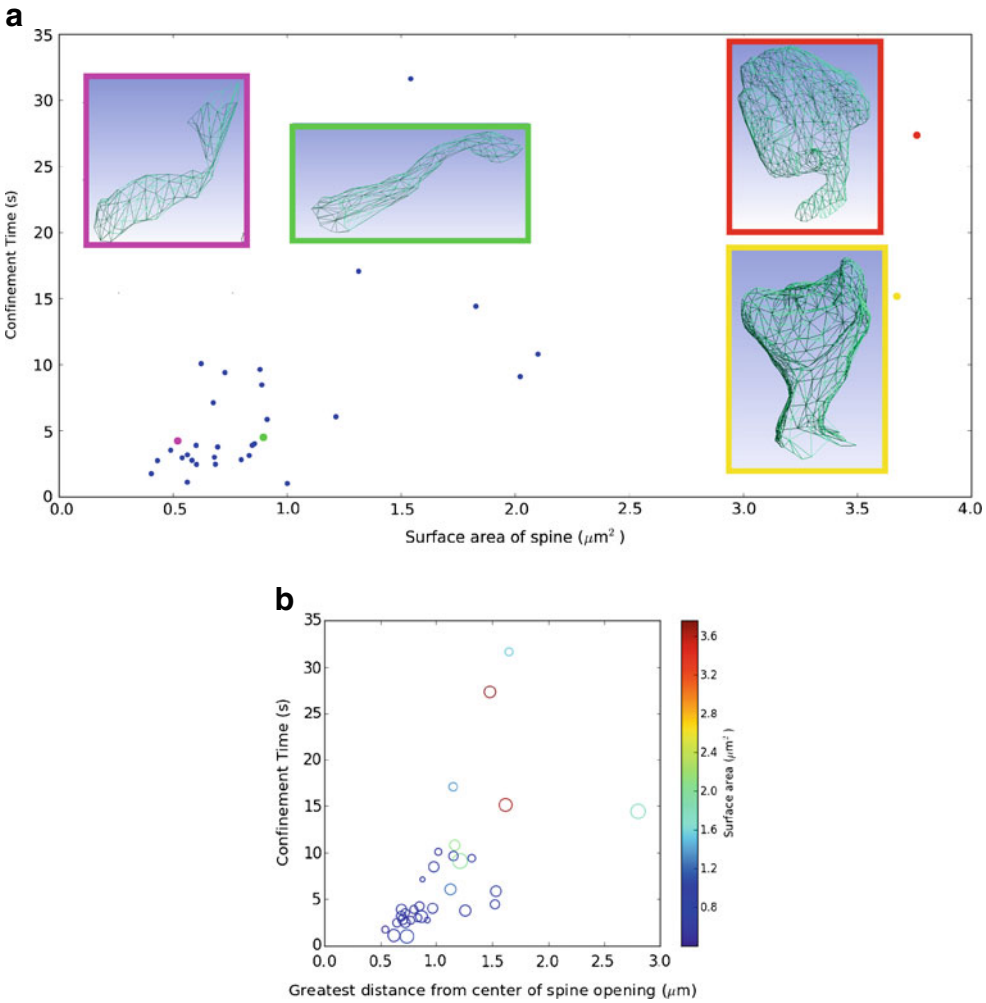

Fig. 3 Geometric relationships. **a** Confinement time correlates positively with surface area. By comparing spines with similar surface area but different confinement times (e.g., K21.1 in red vs. K21.3 in yellow) or similar confinement times but different surface areas (e.g., K21.6 in pink and K21.2 green), we see that a constricted spine neck helps compartmentalize receptors. **b** Confinement time correlates positively with a metric of spine length– the greatest distance of a point on the spine surface to the center of the opening onto the dendrite. Each spine is a point. The radius of the point is proportional to the radius of the opening onto the spine; the color represents the surface area. The surface area trend in (**a**) can also be visualized here

exit. Fig. 3b serves as a summary of our MFPT data since it includes all three geometric descriptors. The size of the points are proportional to the circumference of the spine opening onto the dendrite; the color denotes the surface area. While we did not find a strong corrleation between the circumference of the spine opening with the confinement time, we can understand violations of the length-confinement time trend by considering the circumference of the opening. The spine with by far the largest length does not have the largest confinement time because its opening onto the dendrite is very large, inviting the receptor to exit. Several spine pairs have similar lengths and surface areas, but a larger opening in one reduces the confinement time below the other. The spine with the largest confinement time has a relatively large surface area and length– but not the largest– and a small opening, serving as a key resistance to exit. These three, simple spine geometry descriptors provide intuition in understanding why one spine is endowed with a higher MFPT than another. However, a spine geometry is obviously not fully determined by these three descriptors.

We visualize the MFPT as a function of the initial position y in Fig. 4. The MFPT is low in regions close to the spine neck boundary since the particle starts off close to the trapping region, while further away the MFPT is higher. The maximum MFPT:

$$\max_y \bar{\tau}_{(y)}, \tag{14}$$

yields the highest capability of the spine to compartmentalize a receptor by maximizing over all possible initial conditions. The white spheres in Fig. 4 are the points y on the spine at which the maximum MFPT occurs. Also in Fig. 4 we compare the location of the maximum MFPT to the location of the excitatory synapse region (indicated in red) in a sample of spines. For most spines, the location of the maximum MFPT corresponds closely to the location of the excitatory synaptic region (distance 0.14 ± 0.07 μm, $n = 14$). A spine can maintain ownership of a receptor and maximizes the residence time of a diffusing receptor by placing it at the location at which the maximum MFPT occurs.

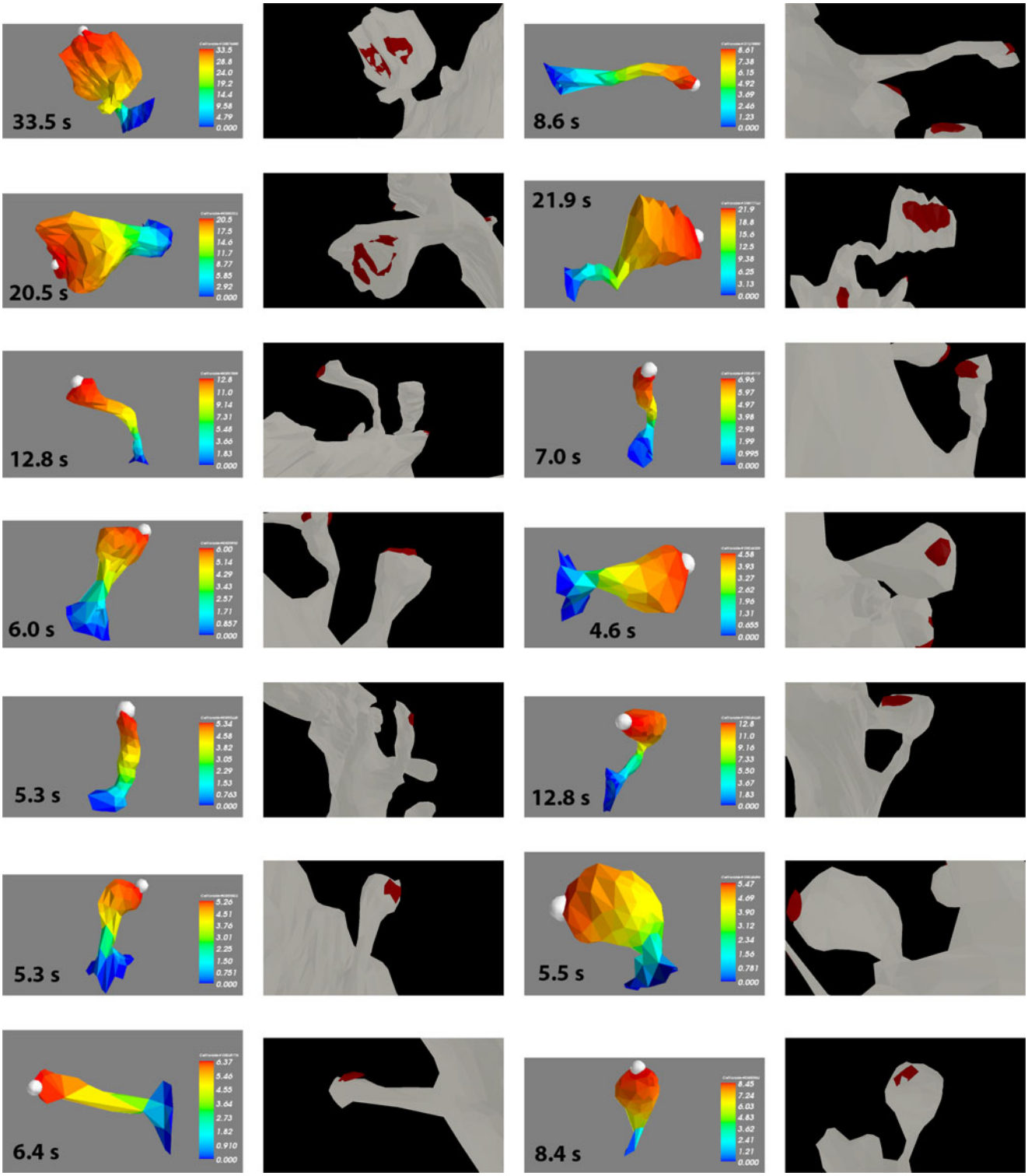

Fig. 4 The MFPT $\bar{\tau}_{(y)}$ (s) as a function of the initial position y on Ω_s (colorbar) next to the image of the spine on the dendrite with the excitatory postsynaptic density indicated in red. The maximum of the MFPT is indicated by the white sphere for comparison to the location of the synaptic region. Maximum MFPT is written in black text. Note: the spatial scales are not the same for each figure. (Images from dendrite K21)

Defining $\max_y \bar{\tau}_{(y)}$ as a metric for compartmentalization of receptors, the correlation between spine surface area and compartmentalization still holds. Figure 5 relates $\max_y \bar{\tau}_{(y)}$ and the confinement time T by overlaying the two

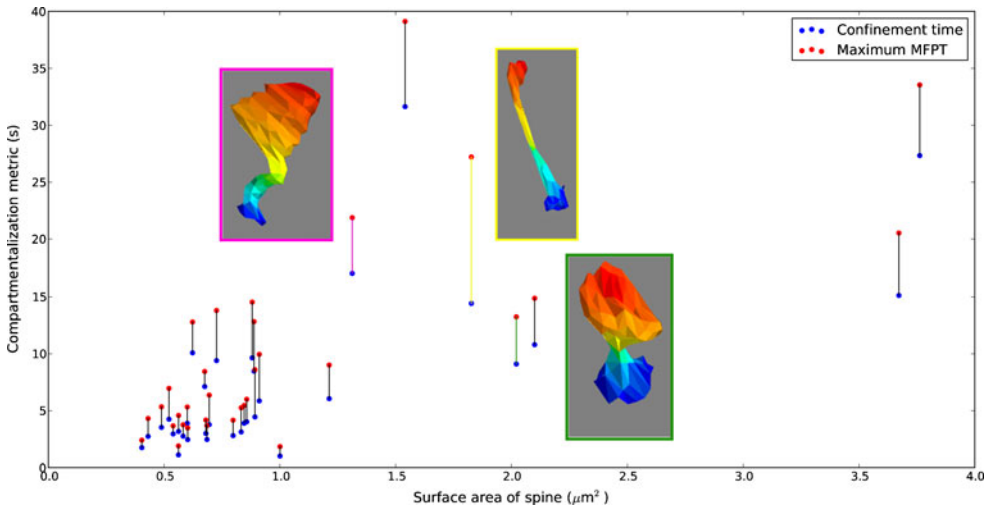

Fig. 5 Comparing two metrics of receptor compartmentalization: confinement time T and maximum MFPT $\bar{\tau}_{(y)}$. Spine K18.1 (*yellow*) has a greater difference between the maximum MFPT and confinement time than the bulbous spine K18.2 (*green*) despite having less surface area because it has a broader distribution of distances from the trapping region due to its long, skinny morphology. Conclusions of which spine is more suitable for compartmentalizing receptors switch for spine K21.4 (*pink*) and K18.1 depending which metric is used

scatter plots with respect to surface area and connecting the points corresponding to the same spine with a line. It is instructive to consider the differences between the $\max_y \bar{\tau}_{(y)}$ and T as a function of spine surface area. The trend is that $\max_y \bar{\tau}_{(y)} - T$ increases with surface area because, given a typical shape, there is a wider distribution of distances from the trapping region in larger spines than smaller ones. Spine K18.2 (green) has a greater surface area than spine K18.1, yet it yields a lesser $\max_y \bar{\tau}_{(y)} - T$, violating the trend. Comparing the morphologies, we see that spine K18.1 is long and skinny compared to the bulbous spine K18.2, yielding a wider distribution of distances from the trapping region despite having less surface area. Spine K18.1 (yellow) and spine K21.4 (pink) follow this trend, and it causes a discordance in the conclusions of which spine is better at retaining receptors. Using the confinement time metric, spine K21.4 is better at compartmentalizing receptors than spine K18.1. However, using the maximum MFPT as a metric, the spine K18.1 has a greater ability to compartmentalize receptors when it places a receptor at the very tip, which is a larger distance from the trapping region than possible in spine K21.4. Thus, choosing a metric to determine which spine shape is more suitable for compartmentalizing receptors depends on the criterion (i) maximum potential for compartmentalizing a single receptor (use $\max_y \bar{\tau}_{(y)}$) or (ii) considering all possible receptor positions (use T).

Finally, we compare our approach of computing the MFPT on realistic spine geometries to an analytical formula that idealizes a spine as a sphere of radius R_s connected orthogonally to a cylinder of radius R_c and length L. From (Holcman and Schuss 2011), a formula for the maximum MFPT for a diffusing particle to exit through the cylinder yields insight into how particular parameters influence the MFPT:

$$\max_y \bar{\tau} = \frac{2R_s^2}{D} \log\left(\frac{R_c}{R_s}\right) + \frac{L_c^2}{2D} + \frac{2R_s^2 L_c}{R_c D}. \tag{15}$$

We choose the spine in Fig. 1b that most resembles a cylindrical neck connected orthogonally to a spherical head for comparison. We partition the point cloud representation of the spine into a neck and head point set and fit a cylinder and sphere, respectively, to the point cloud (see Materials and Methods) to determine R_c, R_s, and L (see Fig. 6a). Using formula 15 with the parameters from the fitted cylinder and sphere, we calculate $\max_y \bar{\tau} \approx 5.7$ s, whereas $\max_y \bar{\tau}$ is computed as approximately 6.2 s using the finite volume method and the triangulated sphere surface– a 17 % error (using the finite volume method on the triangulated surface as a basis). Geometric idealization of another spine (Fig. 6b) with less resemblance to a cylinder orthogonally intersecting a sphere results in a 27 % error. On the other hand, some spines (e.g., Fig. 6c) are not of a reasonable resemblance to a sphere connected to an orthogonally intersecting cylinder to apply formula (15). In summary, the analytical formulas for idealized geometries can yield a significant error and are, in some cases, an inappropriate representation of the geometry.

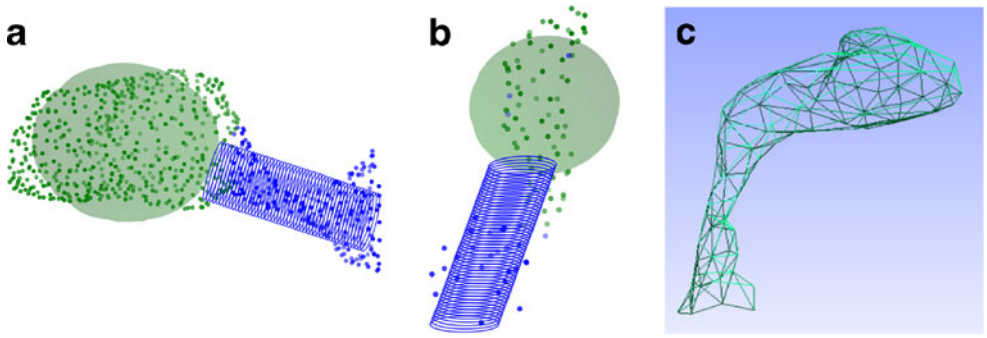

Fig. 6 **a** An idealized representation of the spine in Fig. 1b. We fit a sphere (*green*) and orthogonally intersecting cylinder (*blue*) to the point cloud that represents the spine surface. The green and blue points are the partitions resulting from the clustering algorithm. A 17 % error in the maximum MFPT results from the idealization. **b** A 27 % error in the maximum MFPT results in the geometric idealization of this spine. **c** This spine is not well-represented by a sphere with an orthogonally intersecting cylinder

3 Part II: Delivering AMPARs to excitatory synapses via lateral diffusion following insertion onto the dendritic shaft

Here, we consider when a receptor is inserted at a point y in the plasma membrane of the dendritic shaft and subsequently laterally diffuses on the surface until reaching a synaptic region.

3.1 Model

For time $t = 0$ corresponding to when the receptor is inserted, Ω_d representing the entire dendrite domain, and $\Omega_{PSD} \subset \Omega_d$ representing the region of the spines where the post-synaptic density is located, the evolution of the probability density $p\ (x,\ t)$[1] of finding the particle is governed by:

$$\begin{aligned} \frac{\partial p}{\partial t} &= D\nabla_s^2 p\ ,\ x \in \Omega_d,\ t > 0 \qquad (16)\\ p(x,t) &= 0\ ,\ x \in \Omega_{PSD}\\ p(x,0) &= \delta(x-y). \end{aligned}$$

The dendrite mesh Ω_d is a closed surface, so no boundaries other than Ω_{PSD} are present. The PDE is numerically solved on a reconstructed dendrite image (Harris 2012) with 21 spines. The PSD regions were cut from each spine, and the imposed zero boundary condition at the PSD boundary region models the trapping/absorbing of receptors.

We denote the PSD of the ith spine by $\Omega_{PSD,i}$ such that $\Omega_{PSD} = \cup_i \Omega_{PSD,i}$. We compute the probability that the receptor inserted at y was delivered to the PSD of spine j by time t, $f_j(t;\ y)$, by integrating the flux through the PSD over time:

$$f_j(t;\ y) := -\int_0^t \int_{\partial\Omega_{PSD,i}} D\nabla_s p(x,T)\cdot n dl_x dT, \qquad (17)$$

where n is the outward unit normal vector from the boundary. The probability that the receptor is still diffusing and has not reached a PSD trapping region at time t is the survival function $s(t)$ (Schuss 2010):

$$s(t) := \int_{\Omega_d} p(x,t) dS_x. \qquad (18)$$

Thinking in ensembles, one can interpret $f_j(t;\ y)$ as the fraction of a pool of receptors inserted at y that spine j will receive up to time t and $s(t)$ as the fraction of the receptors that will not have been absorped up to time t.

After a sufficient time, when it is probable that the diffusing receptor has reached a PSD, the distribution $F_j(y) := f_j(t \to \infty;\ y)$ indicates the probability that spine j will receive a receptor inserted at y. Instead of solving Eq. (16) and peforming the integration (17) for a sufficiently long time, the distribution $F_j(y)$ is found by solving a time-independent PDE (Schuss 1980):

$$\begin{aligned} \nabla_s^2 F_j &= 0\ ,\ y \in \Omega_d \qquad (19)\\ F_j(y) &= 1\ ,\ y \in \Omega_{PSD,j}\\ F_j(y) &= 0\ ,\ y \in \Omega_{PSD,i\neq j}. \qquad (20) \end{aligned}$$

Note that the $(t \to \infty)$ distribution of an ensemble of inserted receptors among the spines is independent of the diffusion coefficient. The quantity

$$\left\langle F_j(y)\right\rangle_\Omega = \frac{1}{|\Omega|}\int_\Omega F_j(y) dy, \qquad (21)$$

[1] The quantity $p\ (x,\ t)\ dx$ is the probabiliy of finding the particle in a surface element dx centered at x at time t.

is the probability that spine j will receive a receptor inserted at a random location on the membrane subdomain Ω. This quantity will play a role in determining how spine shape affects the recruitment of receptors.

3.2 Results

We first study a hypothetical case to compare the efficiency of receptor delivery by lateral diffusion from a region on the dendritic shaft, close to the spine, to the ideal case of delivery by insertion from the cytoplasm right next to the PSD. We address the following question regarding the precision of receptor delivery: given an insertion point on the membrane close to a spine, what is the probability that the receptor is received by the intended spine PSD? The answer will depend upon how close the insertion point is to the spine, the spine morphology, and neighboring spines' proximities and morphologies.

It is instructive to simulate three different insertion points (adjacent to the PSD, on the spine neck some distance from the PSD, and on the dendrite shaft next to the spine) with the intention to deliver a receptor to the PSD of spine K21.6, whose boundary is shown in green in Fig. 7. We thrice numerically solve Eq. (16) with y being these points.

Using a diffusion coefficient $D = 0.08\ \mu\text{m}^2/\text{s}$ measured outside of the synapse (Renner et al. 2009), the time scale for a diffusing receptor to reach a spine PSD from the dendrite shaft in our simulations is biologically relevant. Intuitively, the survival function $s(t)$ (right column of Fig. 7) decays more rapidly for the insertion point close to the PSD of spine K21.6 than the one further away. For an insertion point on the dendritic shaft next to spine K21.6, it takes on the order of one minute for a receptor to reach a PSD ($t : s(t) \approx 0.05$).

Figure 7 highlights how a thin, narrow spine neck, while good for compartmentalizing receptors (Part I), hinders the precision in delivering receptors to the PSD via lateral diffusion of receptors inserted onto the dendritic shaft. When the insertion point is close to the PSD of spine K21.6 (Fig. 7, top row), the receptor is delivered to its PSD with 92 % probability. For an insertion point further down the neck of spine K21.6 (Fig. 7, middle row), the PSD of the intended spine K21.6 receives the receptor with 43 % probability, and with 15 % probability the receptor is delivered to the nearby, stubby spine K21.2 (red). For an insertion point on the dendritic shaft next to spine K21.6 (Fig. 7, bottom row), K21.6 receives the receptor with only 14 % probability, whereas the nearby stubby spine K21.2 receives the receptor with 25 % probability. Here, the short, stubby spine K21.2, poor at compartmentalizing receptors (see Fig. 3a), receives an inserted receptor on the dendrite shaft with greater probability than the intended spine K21.6.

To see how the probability that spine K21.6 receives a receptor inserted at y continuously changes with y, we numerically solve Eq. (19) for $F_{K21.6}(y)$ in Fig. 8a. Spine K21.6 has a twisted, highly-constricted neck, and, as a result, the probability that an inserted receptor is absorbed by the PSD decays rapidly as the insertion point moves down the spine. In contrast, spine K21.3 in Fig. 8b, whose PSD is accessible and of a large radius, visibly encompasses a larger region over which an inserted receptor is likely to be absorbed by its PSD. Thus, a constricted spine neck and a smaller and less accessible PSD location can hinder the delivery of AMPA receptors to spines via lateral diffusion after insertion into the dendritic shaft, in contrast to how these factors help compartmentalize these receptors (Part 1).

Next, we consider the more biologically relevant case of an ensemble of AMPA receptor insertions at random locations on the dendrite shaft, but not on the spines themselves (Yudowski et al. 2007; Andrsfalvy et al. 2003). We model Eq. (16) on dendrite K21, but now subject to the initial condition:

$$p(x,0) = \begin{cases} \dfrac{1}{|\Omega_{\text{ds}}|}, & x \in \Omega_{\text{ds}} \\ 0, & x \notin \Omega_{\text{ds}} \end{cases} \tag{22}$$

which is a uniform probability density of insertion over the dendrite shaft (denoted by 'ds'), but not on the spines (see Fig. 9a). We numerically solve Eq. (16) subject to the above initial condition. The survival function $s(t)$, shown in Fig. 9c, decays to 0.05 in ~ 1 min, indicating the time scale for a receptor inserted on the dendritic shaft to reach a spine PSD. For the final distribution of spines, we solve Eq. (20) for $F_j(y)$ and then find $\langle F_j(y)\rangle_{\Omega_{\text{ds}}}$. Any deviation of the distribution $\langle F_j\rangle_{\Omega_{\text{ds}}}$ from a uniform distribution is attributed to geometrical influences. Figure 9b shows that the distribution $\langle F_j\rangle_{\Omega_{\text{ds}}}$ deviates substantially from a uniform distribution, revealing that spine/PSD geometry plays a significant role in receptor recruitment following the insertion of a diffusing receptor on the dendrite shaft.

The stubby spines K21.2 and K21.17 receive the largest fraction of the receptors since their PSD is close to the insertion region and easily accessible from the dendrite shaft. Spines K21.8 and K21.3 receive the next largest fraction of receptors because of their thick necks and PSD boundaries of large circumference (which makes their PSD more accessible as well). Spines K21.18 and K21.7 receive the least amount of receptors. In accordance with Fig. 8a, both of these spines have long, twisted, constricted spine necks, inhibiting their uptake of receptors. Other factors play a role in the distribution $\langle F_j\rangle_{\Omega_{\text{ds}}}$, such as the number of nearby spines to compete for receptors and the length that a spine protrudes from the dendrite, since the spine PSD is then further from the insertion site.

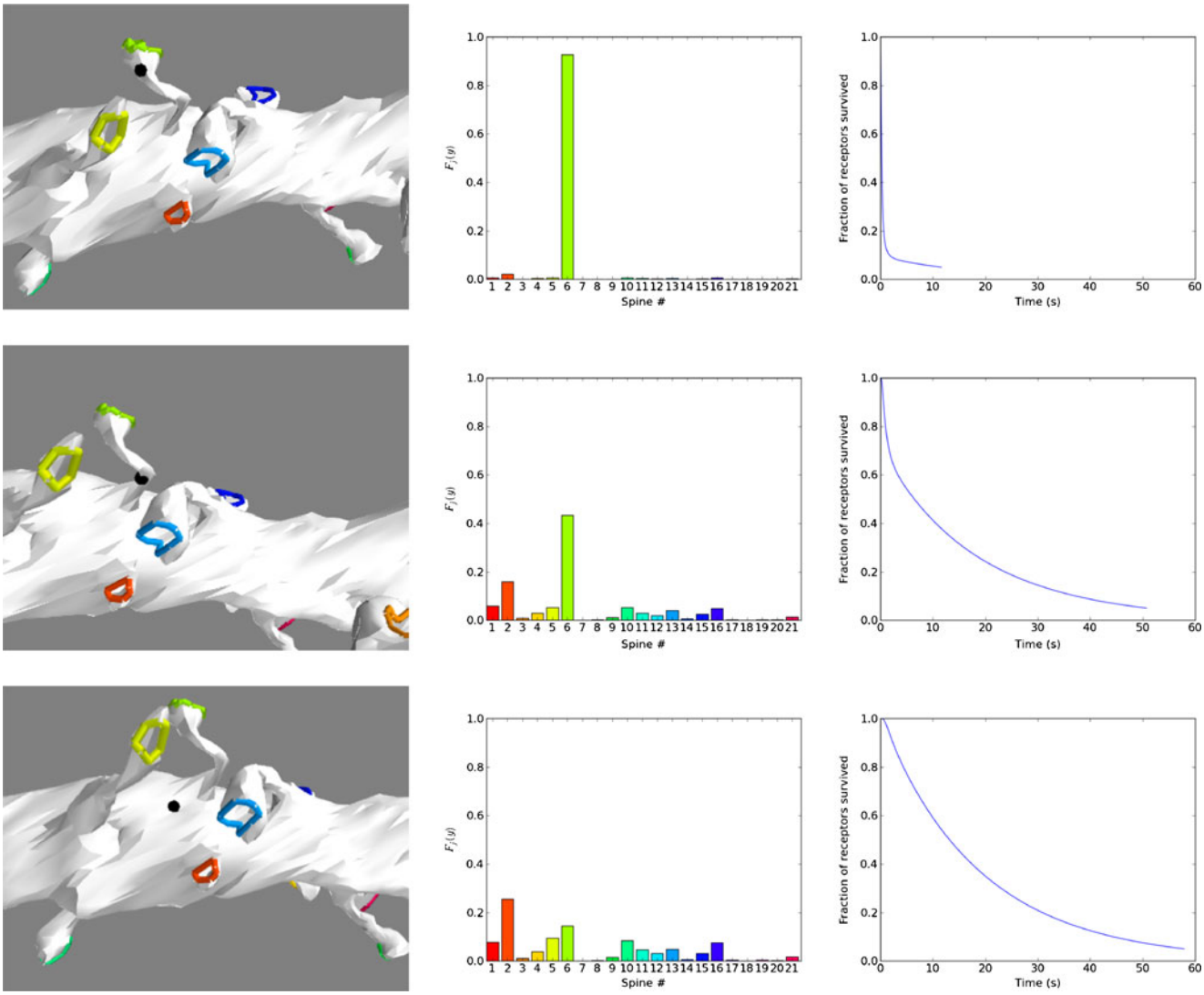

Fig. 7 Precision of receptor delivery to the spine K21.6 (*green*). Top row: Insertion point near PSD. Middle row: Insertion point on spine neck, but a distance from the PSD. Bottom row: Insertion point on dendrite shaft close to the spine. (Col 1) The location y of the insertion point of receptors is shown with the black sphere. (Col 2) The bar graph of the fraction of receptors F_j from the insertion point that are ultimately absorbed by each spine PSD. Colors correspond to the spine colors in Col 1. (Col 3) The survival function $s(t)$ defined in Eq. (18)

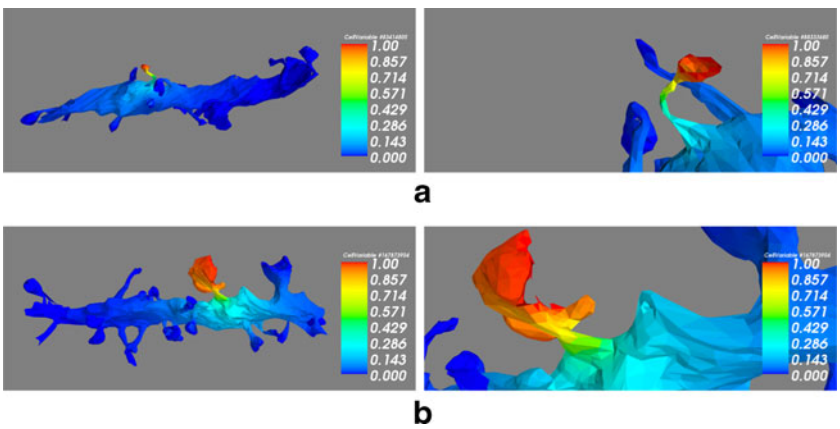

Fig. 8 Distribution $F_j(y)$ for j =K21.6 (**a**) and j =K21.3 (**b**). Right panel is zoomed-in version of left panel. Contrast spine K21.6 (small radius PSD, constricted, twisted neck) to spine K21.6 (large radius PSD, thick neck). The region over which an inserted receptor is likely to be absorbed by the PSD of K21.6 is greater than that of K21.3

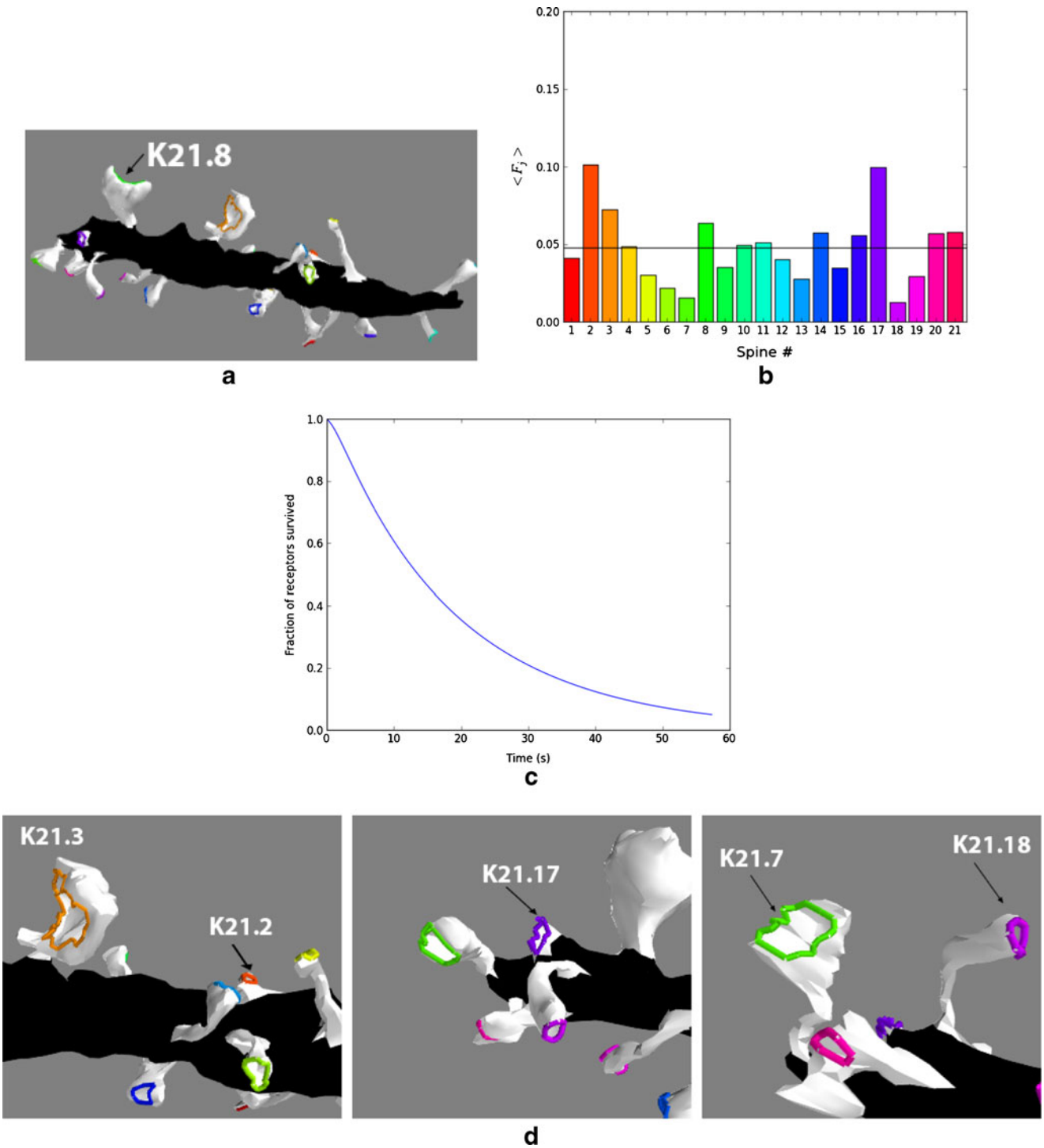

Fig. 9 How spine shape and PSD area affect distribution $\langle F_j \rangle_{\Omega_{ds}}$. **a** A uniform insertion of receptors along the dendrite shaft. The initial condition is constant on the black surface. **b** The distribution $\langle F_j \rangle_{\Omega ds}$ of the receptors among the spines deviates substantially from a uniform distribution, revealing that spine/PSD geometry plays a large role in receptor recruitment. **c** The survival function $s(t)$. **d** Labeling of spines

Discussion

AMPA receptors are major molecular players in synaptic plasticity (Lynch and Baudry 1984; Choquet 2010), and surface diffusion processes on the complex dendritic morphologies affect their presence in synaptic regions. Therefore, it is important to study AMPAR movement and quantity diffusion timescales in realistic neuronal geometries, where reduction to simple geometry primitives, such as cylinders and spheres, can introduce significant errors.

While a subpopulation of the AMPARs are immobile (Giannone et al. 2010), a substantial fraction are mobile (Ashby et al. 2006; Heine et al. 2008). Previous works have attempted analytical solutions and approximations to the MFPT problem in the context of dendritic spines (Holcman and Schuss 2004; Schuss et al. 2007; Holcman and Schuss 2011; Holcman et al. 2006). To our knowledge, our work is the first computer simulation of the Dykin's MFPT PDE and the distribution F_j of the receptor exit points on a sample of real dendritic spine morphologies. We studied how the spine morphology affects two processes, both involving lateral diffusion of receptors: (1) compartmentalizing the surface receptors in a single spine to retain local AMPAR density and (2) the delivery of new receptors to the PSD of spines by lateral diffusion following insertion onto the dendrite.

In Part I, we computed the MFPT of AMPA receptors on the surface of 33 dendritic spine samples. We found the median confinement time (max MFPT) to be $\sim$4 ($\sim$6) s, giving a time scale for the residence time of AMPARs on the spine in the absence of protein scaffolds or lipid rafts interfering with lateral diffusion. The average MFPT (the confinement time) and the maximum MFPT can lead to opposite conclusions on which spine is best at compartmentalizing. The maximum MFPT is a better metric for considering the maximum potential for a spine to compartmentalize the receptors by strategically placing the particle furthest from the neck. We investigated the spines' geometric relationships with the MFPT by computing the effective length, surface area, and circumference of the opening. The MFPT positively correlates with surface area and effective length. In the instructive process of comparing spine morphologies on the effective length- and surface area- compartmentalization scatter plots, we confirm that, in accordance with several other works, a constricted spine neck (small circumference of opening) serves to compartmentalize receptors. We found that the location of the PSD closely follows that of the location at which the maximum MFPT occurs, which is where a neuron would evolve to place its receptors to maximize receptor residence time on the spine.

In Part II, we considered the delivery of receptors to PSD sites by lateral diffusion following the insertion of a receptor on the shaft of the dendrite. Simulating diffusion on the dendrite surface and subsequent absorption into the PSD regions, we found the time-scale of delivery to be one minute. The probability that a receptor is delivered to a particular spine is an interplay between the insertion site, the shape of the spines and their locations on the dendrite, and the shape and location of the PSD on each spine. In Part I, a highly constricted spine neck and a PSD that is located at the point at which the maximum MFPT occurs are effective in compartmentalizing receptors in the spine. However, these same properties render a spine less effective in recruiting receptors that were inserted into the dendritic shaft. An ensemble of random insertion locations of receptors indicates that spines with the most constricted necks receive less receptors in comparison to large, easily-accessible PSDs. This suggests that the 'optimal' spine morphology depends upon the intention to recruit laterally diffusing receptors on the dendrite or to keep the current receptor pool from diffusing away. For example, short, stubby spines are particularly effective at recruiting receptors inserted on the dendritic shaft.

For real cells, there are departures from the classical fluid-mosaic model by Singer and Nicolson (Singer and Nicolson 1972), where cellular membranes are fluid and characterized by random distributions of molecular components in the membrane. The most significant extrasynaptic contributor to heterogeneity is the presence of lipid rafts, though other features can contribute such as protein traps and obstacles and anchoring to the submembrane cytoskeleton (Triller and Choquet 2008). While there is high uncertainty in the fraction of cell surface covered by lipid rafts and considerable variation between different cell types, published values of coverage for different cell types using different experimental techniques estimate raft coverage from a few percent to as high as 50 % (Simons and Toomre 2000; Pike 2003). However, in neurons, lipid rafts accumulate mostly in the axonal plasma membrane (Simons and Toomre 2000) (which we are not concerned with in this study); they do exist in dendritic membranes but in much smaller amounts (Simons and Toomre 2000), suggesting that dendritic membranes are much more homogeneous than axonal membranes. Supporting this, experimental observations of molecular movements in extrasynaptic regions show that movement is highly Brownian (Triller and Choquet 2008; Tardin et al. 2003; Renner et al. 2009) (whereas in synaptic regions it is not), giving strong evidence that the assumption of homogeneity in extrasynaptic regions is a good approximation. Nonetheless, including receptor trapping would necessarily increase the MFPT since AMPARs would now have to overcome the extra obstacles to exit the spine; thus, our Brownian diffusive timescales are lower bounds.

Future work involves more realistic diffusion models that include scaffolding (Choquet and Triller 2003) and non-Brownian surface receptor movement (Borgdorff and Choquet 2002). The two themes of compartmentalization and spine delivery to the PSD can be amalgamated by modeling receptors exiting the PSD with a Robin boundary condition (Bressloff and Earnshaw 2007) instead of a perfectly absorbing, zero boundary condition in this work. With recruitment and compartmentalization properties defined for realistic spine morphologies, it may be possible to confer how spine shape changes (Fischer et al. 1998) might reflect adaptations to the intention to recruit or retain receptors.

Conflict of interests No conflict of interests declared.

References

Andrsfalvy, B.K., Smith, M.A., Borchardt, T., Sprengel, R., Magee, J.C. (2003). Impaired regulation of synaptic strength in hippocampal neurons from glur1-deficient mice. *The Journal of Physiology*, *552*(1), 35–45.

Ashby, M., Maier, S., Nishimune, A., Henley, J. (2006). Lateral diffusion drives constitutive exchange of ampa receptors at dendritic spines and is regulated by spine morphology. *Journal of Neuroscience*, *26*(26), 7046–7055.

Biess, A., Korkotian, E., Holcman, D. (2007). Diffusion in a dendritic spine: The role of geometry. *Physical Review E*, *021922*, 76.

Borgdorff, A., & Choquet, D. (2002). Regulation of ampa receptor lateral movements. *Nature*, *417*, 649–653.

Bressloff, P.C., & Earnshaw, B.A. (2007). Diffusion-trapping model of receptor trafficking in dendrites. *Physical Review E*, *75*(041915).

Calhoun, D., & Helzel, C. (2009). A finite volume method for solving parabolic equations on logically cartesian curved surface meshes. *SIAM Journal on Scientific Computing*, *31*(6).

Cautres, R., Herbin, R., Hubert, F. (2004). The lions domain decomposition algorithm on non matching cell-centered nite volume meshes. *IMA Journal of Numerical Analysis*, *24*(3), 465–490.

Choquet, D. (2010). Fast ampar trafficking for a high-frequency synaptic transmission. *European Journal of Neuroscience*, *32*, 250–260.

Choquet, D., & Triller, A. (2003). The role of receptor diffusion in the organization of the postsynaptic membrane. *Nature Reviews Neuroscience*, *4*, 251–265.

Dyhkin, E.B. (1965). Markov Processes I,II, Springer Verlag.

Ehlers, M.D., Heine, M., Groc, L., Lee, M.-C., Choquet, D. (2007). Diffusional trapping of glur1 ampa receptors by input-specific synaptic activity. *Neuron*, *54*(3), 447–460.

Fischer, M., Kaech, S., Knutti, D., Matus, A. (1998). Rapid actin-based plasticity in dendritic spines. *Neuron*, *20*(5), 847–854.

Geuzaine, C., & Remacle, J.-F. (2009). Gmsh: a three-dimensional finite element mesh generator with built-in pre- and post-processing facilities. *International Journal for Numerical Methods in Engineering*, *79*(11), 1309–1331.

Giannone, G., Hosy, E., Levet, F., Constals, A., Schulze, K., Sobolevsky, A., Rosconi, M., Gouaux, E., Tamp, R., Choquet, D., Cogne, L. (2010). Dynamic superresolution imaging of endogenous proteins on living cells at ultra-high density. *Biophysical Journal*, *99*(4), 1303–1310.

Guyer, J.E., Wheeler, D., Fipy, Warren, J.A. (2009). Partial differential equations with python. *Computing in Science and Engineering*, *11*(3), 6–15.

Harris, K.M.(P.I.). (2012). Synapse web. http://synapses.clm.utexas.edu/anatomy/Ca1pyrmd/radiatum/index.stm. See K21 and K18.

Harris, K.M., & Stevens, J.K. (1989). Dendritic spines of ca1 pyramidal cells in the rat hippocampus: serial electron microscopy with reference to their biophysical characteristics. *Journal of Neuroscience*, *9*, 2982–2997.

Heine, M., Groc, L., Frischknecht, R., Bque, J.C., Lounis, B., Rumbaugh, G., Huganir, R., Cognet, L., Choquet, D. (2008). Surface mobility of postsynaptic ampars tunes synaptic transmission. *Science*, *320*(5873), 201–205.

Holcman, D., & Schuss, Z. (2004). Escape through a small opening: Receptor trafficking in a synaptic membrane. *Journal of Statistical Physics*, *117*(5/6), 975–1014.

Holcman, D., & Schuss, Z. (2011). Diffusion laws in dendritic spines. *Journal of Mathematical Neuroscience*, *1*(10).

Holcman, D., Korkotian, E., Segal, M. (2005). Calcium dynamics in dendritic spines, modeling and experiments. *Cell Calcium*, *37*(5), 467–475. Calcium in the function of the nervous system: New implications.

Holcman, D., Singer, A., Schuss, Z. (2006). Narrow escape, part ii: The circular disk. *Journal of Statistical Physics*, *122*(3), 465–489.

Holmes, W.R. (1990). Is the function of dendritic spines to concentrate calcium? *Brain Research*, *519*(1-2), 338–342.

Hugel, S., Abegg, M., de Paola, V., Caroni, P., Gahwiler, B., McKinney, R. (2009). Dendritic spine morphology determines membrane-associated protein exchange between dendritic shafts and spine heads. *Cerebral Cortex*, *19*(3), 697–702.

Jaskolski, F., & Henley, J.M. (2009). Synaptic receptor trafficking: The lateral point of view. *Neuroscience*, *158*, 19–24.

Kieri, E. (2011). Accuracy aspects of the reaction-diffusion master equation on unstructured meshes. Uppsala Universitet.

Lynch, G., & Baudry, M. (1984). The biochemistry of memory: A new and specific hypothesis. *Science*, *224*, 1057–1063.

Makino, H., & Malinow, R. (2009). Ampa receptor incorporation into synapses during ltp: the role of lateral movement and exocytosis. *Neuron*, *64*, 381-390.

Masugi-Tokita, M., Tarusawa, E., Watanabe, M., Molnár, E., Fujimoto, K., Shigemoto, R. (2007). Number and density of ampa receptors in individual synapses in the rat cerebellum as revealed by sds-digested freeze-fracture replica labeling. *The Journal of Neuroscience*, *27*(8), 2135–2144.

Newpher, T.M., & Ehlers, M.D. (2008). Glutamate receptor dynamics in dendritic microdomains. *Neuron*, *58*(4), 472–497.

Nicholson, D., Trana, R., Katz, Y., Kath, W., Spruston, N., Geinisman, Y. (2006). Distance-dependent differences in synapse number and ampa receptor expression in hippocampal ca1 pyramidal neurons. *Neuron*, *50*, 431–442.

Noguchi, J., Matsuzaki, M., Ellis-Davies, G.C.R., Kasai, H. (2005). Spine-neck geometry determines nmda receptor-dependent ca2+ signaling in dendrites. *Neuron*, *4*, 609–622.

OBrien, R.J., Kamboj, S., Ehlers, M.D., Rosen, K.R., Fischbach, G.D., Huganir, R.L. (1998). Activity-dependent modulation of synaptic ampa receptor accumulation. *Neuron*, *21*(5), 1067–1078.

Opazo, P., Labrecque, S., Tigaret, C., Frouin, A., Wiseman, P., De Koninck, P., Choquetl, D. (2010). Camkii triggers the diffusional trapping of surface ampars through phosphorylation of stargazin. *Neuron*, *67*(2), 239–252.

Pike, L.J. (2003). Lipid rafts bringing order to chaos. *Journal of Lipid Research*, *44*(4), 655–667.

Renner, M., Choquet, D.l., Triller, A. (2009). Control of the postsynaptic membrane viscosity. *The Journal of Neuroscience*, *29*(9), 2926–2937.

Sabatini, B.L., Maravall, M., Svoboda, K. (2001). Ca(2+) signaling in dendritic spines. *Current Opinion Neurobiology*, *11*(3), 349–56.

Santamaria, F., Wils, S., De Schutter, E., Augustine, G.J. (2006). Anomalous diffusion in purkinje cell dendrites caused by spines. *Neuron*, *52*(4), 635–648.

Schuss, Z. (1980). *Theory and applications of stochastic differential equations*. Wiley.

Schuss, Z. (2010). *Theory and applications of stochastic processes: an analytical approach*. Springer.

Schuss, Z., Singer, A., Holcman, D. (2007). The narrow escape problem for diffusion in cellular microdomains. *PNAS*, *104*(41), 16098–16103.

Sheng, M., & Jong Kim, M. (2002). Postsynaptic signaling and plasticity mechanisms. *Science*, *298*(25), 776–780.

Sheng, M., & Lee, S.H. (2001). Ampa receptor trafficking and the control of synaptic transmission. *Cell*, *105*(7), 825–828.

Simons, K., & Toomre, D. (2000). Lipid rafts and signal transduction. *Nature Reviews Molecular Cell Biology*, *1*(1), 31–39.

Singer, S.J., & Nicolson, G. (1972). The fluid mosaic model of the structure of cell membranes. *Science*, *175*(4023), 720–731.

Svoboda, K., Tank, D.W., Denk, W. (1996). Direct measurement of coupling between dendritic spines and shafts. *Science*, *272*(5262), 716–719.

Tardin, C., Cognet, L., Bats, C., Lounis, B., Choquet, D. (2003). Direct imaging of lateral movements of ampa receptors inside synapses. *The EMBO Journal*, *22*(18), 4656–4665.

Triller, A., & Choquet, D. (2008). New concepts in synaptic biology derived from single-molecule imaging. *Neuron*, *59*(3), 359–374.

Yudowski, G.A., Puthenveedu, M.A., Leonoudakis, D., Panicker, S., Thorn, K.S., Beattie, E.C., von Zastrow, M. (2007). Real-time imaging of discrete exocytic events mediating surface delivery of ampa receptors. *The Journal of Neuroscience*, *27*(41), 11112–11121.